Available online at www.sciencedirect.com

ScienceDirect

Advances in Space Research 56 (2015) 2432–2438

ADVANCES IN SPACE RESEARCH (a COSPAR publication)

www.elsevier.com/locate/asr

Work function measurements of olivine: Implication to photoemission charging properties in planetary environments

Hong Gan [a,b], Xiongyao Li [a,*], Guangfei Wei [a], Shijie Wang [c]

[a] Lunar and Planetary Science Research Center, Institute of Geochemistry, Chinese Academy of Sciences, Guiyang 550081, China
[b] University of Chinese Academy of Sciences, Beijing 100049, China
[c] State Key Laboratory of Environmental Geochemistry, Institute of Geochemistry, Chinese Academy of Sciences, Guiyang 550081, China

Received 8 May 2015; received in revised form 2 September 2015; accepted 5 October 2015
Available online 13 October 2015

Abstract

For understanding the ubiquitous photoemission charging of solid surface in planetary environments, it is important to characterize the photoemission charging properties of silicate minerals such as the work function. In this study, we measured the work function of olivine mineral based on the measurements of contact potential difference by using an ultrahigh vacuum Kelvin probe force microscopy. Our results showed that work function on olivine mineral surface is mainly affected by surface morphology and crystal orientation and that the variation range of work function is 7.3–8.5 eV. It implicates that photoemission of the olivine mineral occurs under the X-ray and solar ultraviolet irradiation with wavelength of <171 nm. Consequently, it is possible to form electrostatic field of +(5–10) V on the sunlit planet, moon or asteroid surfaces due to dust photoemission charging, which even induces the migration of dust grains and the formation of dust-plasma atmosphere. Those are important problems worried to be solved for future lunar missions. Additionally, our work can help to instruct the dust mitigation technology and the electrostatic beneficiation in future space missions.

Keywords: Planet; Moon; Photoemission; Olivine; Work function

1. Introduction

The photoemission of lunar regolith induced by solar ultraviolet and X-ray radiation is one of the main reasons for creating the electrostatic field in the near-surface of the Moon. On the dayside of the Moon, the surface typically charges positive (~+10 V) because the current generated by the photoemission dominates (Manka, 1973; Freeman and Ibrahim, 1975; Colwell et al., 2007). This charging phenomenon also occurs on the surface of atmosphereless planets (e.g. Mercury) and asteroids, and is responsible for the charging of interplanetary dust grains. In fact, the solid surface exposed directly to the solar radiation acquires a potential of +(5–10) V in space and even a global photoelectron sheath above the sunlit surface (Delory, 2010).

For understanding the photoemission mechanism on the solid surface, work function of materials surface is a key parameter. Up to now, work function has been extensively measured or calculated on metal (Lang and Kohn, 1971; Ekardt, 1984; Fujii et al., 2006), semiconductor (Sadewasser et al., 2002) and even organic materials/devices (Kotani and Akamatu, 1971; Hoppe et al., 2005). However, the work function measurements of insulating materials are rarely reported. Interplanetary dust grains and solid planet surface mostly consist of silicate debris and glasses which are formed by the interaction between these materials and its space environment. These silicate

* Corresponding author. Tel.: +86 189 850 29760.
E-mail addresses: ganhong06@gmail.com (H. Gan), lixiongyao@vip.skleg.cn (X. Li).

http://dx.doi.org/10.1016/j.asr.2015.10.005
0273-1177/

materials mostly belong to insulator. The work function of the solid insulator is defined as the minimum energy required to extract the weakest bound electron from its maximum nature surface excursion distance to infinity (Gallo and Lama, 1976). In 1972, the photoelectric characteristics of lunar surface fines (No. 14259,116) were presented and the sample work function is measured to be about 5 eV (Feuerbacher et al., 1972). Based on the data of the charged particle lunar environment experiment (CPLEE), the work function of lunar surface materials was estimated to 6 eV (Reasoner and Burke, 1972). Additionally, other previous theoretical and experimental results also showed that the work function of lunar surface material exposed to the solar wind is mainly in the range of 5–6 eV (Freeman and Ibrahim, 1975).

However, for the long term of micro-meteorite bombardment and space weathering on the surface of atmosphereless bodies, the regolith becomes mature and contains abundant of agglutinate glasses with the excess nano-phase iron (np-Fe^0), which brings some difficulty for investigating photoemission charging properties of lunar regolith. In addition, the derived work function of lunar regolith (a mixture of minerals and glasses) can not characterize appropriately the crystalline components such as pyroxene, plagioclase and olivine. Therefore, it is necessary to measure the work function of different insulating minerals and glasses for further understanding the photoemission mechanism of typical minerals in the fields of material science and planetary science. In this study, we have measured the work function of olivine, which is a magnesium iron silicate with the formula $(Mg^{+2}, Fe^{+2})_2SiO_4$. Note that olivine is a common mineral within ultramafic rocks and distributed widely in solid planets, moons, meteorites and even planetary rings, comet tails, interplanetary dust particles.

Work function is not a intrinsic characteristic of bulk materials, but a physical property of the materials surface. Many techniques have been developed to measure the work function, such as Ultraviolet photoemission spectroscopy (UPS) (Kötz et al., 1986; Park et al., 1996; Kim et al., 2000), X-ray photoemission spectroscopy (XPS) (Kötz et al., 1986; Park et al., 1996) and Kelvin probe force microscopy (KPFM) (Nonnenmacher et al., 1991; Sommerhalter et al., 1999; Melitz et al., 2011). KPFM is based on contact potential difference method to determine work function of an unknown surface. KPFM has a high spatial resolution and allows the simultaneous imaging of morphology and contact potential difference (CPD) (Melitz et al., 2011). Recently, KPFM is widely applied to measure the work function of various semiconductor and organic materials (Hoppe et al., 2005; Kim et al., 2007; Sadewasser et al., 2009). Here, we employed Kelvin probe force microscopy to measure the work function of the insulator mineral, olivine. Then, we analyzed the effect of surface morphology and crystal orientation on the work function. Furthermore, we calculated the threshold wavelength of the incident photon for the photoelectric effect on olivine surface based on the measurements. This result is conducive to better understand the photoelectric properties of olivine mineral, and it also provides certain constraints for the photoelectric charging and triboelectric charging mechanism of dust grains (Gallo and Lama, 1976; Sickafoose et al., 2000; Sickafoose et al., 2001). It also implicates the formation of surface photoelectron sheath and the law of dust transport in the sheath (Grobman and Blank, 1969; Sternovsky et al., 2008). In addition, it also provides some instructions of the advanced dust mitigation technology and the electrostatic beneficiation in future lunar and Martian exploration (Gupta et al., 1993; Li et al., 1999).

2. Experiment

For characterizing the surface structure and composition of lunar samples and meteorites, we have developed an ultrahigh vacuum (UHV) surface analysis system, which integrates the SPECS Curlew (Berlin, Germany) scanning probe microscope (SPM) with X-ray photoelectron spectroscopy (XPS), auger electron spectroscopy (AES), etc. The major specifications of the SPECS Curlew SPM include that XY scan range of sample is $10 \times 10\ \mu m^2$ and Z scan range of tip is 2 μm. The SPM tip is a quartz tuning fork based the silicon cantilever of atomic force microscope (AFM) sensor (Akiyama probe). Kelvin Controller Module in the Nanonis SPM control system software is used to control Kelvin Probe Imaging. KPFM obtains work function of material surface based on the measurements of the contact potential difference between the sample surface and the AFM probe, which originates from work function difference between two materials. When the two materials remain unconnected, their local vacuum levels are aligned but with different Fermi levels. Once the two materials connect, their Fermi levels will align by electron transfer but there is difference between their local vacuum levels. Their local vacuum levels will be aligned again by compensating an external bias which equals to the CPD in theory. Hence, KPFM measures CPD between the tip and the sample surface, which is determined by

$$V_{CPD} = \frac{\Phi_{tip} - \Phi_{sample}}{-Q} \quad (1)$$

where Φ_{tip} and Φ_{sample} are the work functions of the tip and the sample surface respectively, and Q is the elementary charge. Under a potential difference between the AFM tip and the sample, the electrostatic force is given by

$$F = -\frac{1}{2}\Delta V^2 \frac{\partial C}{\partial z} \quad (2)$$

where C is the capacitance between the tip and the sample and z is the distance between them. ΔV is the potential difference between V_{CPD} and the voltage applied to the AFM tip, which is $\Delta V = V_{tip} \pm V_{CPD}$. Note that the $\pm$ sign depends on the bias applied to the sample (+) or the tip (−). In order to measure V_{CPD}, an AC voltage (V_{AC}) and

a DC voltage (V_{DC}) are applied to the AFM tip. The AC voltage generates oscillating electrical force between the tip and the sample surface, while the DC voltage nullifies the oscillating electrical force from the CPD between the tip and the sample surface. A lock-in amplifier is employed to extract the additional oscillating signal applied to the tip by the V_{AC} and V_{DC}. The V_{CPD} can be obtained when the output signal of the lock-in amplifier is nullified, which indicates the local vacuum levels of the tip and the sample are aligned again.

In our measurements, all data and images were acquired by KPFM based on the technique of an ultrahigh vacuum non-contact atomic force microscope (NC-AFM), which is used for simultaneous observation of the bias and NC-AFM images. Before measuring the local contact potential difference (LCPD) between the tip and the sample, a bias is compensated on the tip by using the Contact Potential Compensation Tool. Based on the average CPD between the tip and each point on the sample surface, the compensated bias is acquired as the CPD value between the tip and the whole scanning area. The LCPD actually is the total values of the CPD and the local bias in rescanning bias image. During imaging process, the vacuum pressure is maintained at less than 10^{-8} Pa. The cantilever has a resonance frequency of 50 kHz and a spring constant of 5 N/m. Both the cantilever and tip are made from n-type silicon (n-Si).

Based on Eq. (1), it is important that the work function of the tip is accurately determined before deriving the work function of olivine. Therefore, the tip was calibrated by two standard samples, Ag and highly oriented pyrolytic graphite (HOPG). The theoretical values of HOPG and Ag work function are 5.0 eV and 4.26 eV, and meet Eqs. (3) and (4), respectively.

$$\Phi_{HOPG} - \Phi_{tip} = QV_{CPD_{HOPG-tip}} \tag{3}$$

$$\Phi_{Ag} - \Phi_{tip} = QV_{CPD_{Ag-tip}} \tag{4}$$

where Φ_{HOPG} and Φ_{Ag} are the work function values of HOPG and Ag, and $V_{CPD_{HOPG-tip}}$ and $V_{CPD_{Ag-tip}}$ are the contact potential difference between the HOPG/Ag surface and the tip. According to Eqs. (3) and (4), we get that

$$V_{CPD_{HOPG-Ag}} = V_{CPD_{HOPG-tip}} - V_{CPD_{Ag-tip}} = \frac{\Phi_{HOPG} - \Phi_{Ag}}{Q} \tag{5}$$

where $V_{CPD_{HOPG-Ag}}$ is the contact potential difference between the HOPG and Ag.

Based on the Eq. 5, the theoretical CPD value between the standard samples HOPG and Ag is 0.74 V. The mean CPD values between HOPG/Ag and the tip measured in our experiment are 0.48 V and −0.23 V, respectively. Therefore, $V_{CPD_{HOPG-Ag}}$ obtained by our measurements is 0.71 V, which approximately equals to the theoretical value of 0.74 V. Here, we chose HOPG as the main reference material in our measurements, for the freshly exposed HOPG has clean surface and stable surface structures. The mean work function values of the tip and the standard sample Ag are determined as 4.52 eV and 4.29 eV, respectively. The average error of the measured work function values for the standard sample Ag is 0.7%, according to $(\Phi^m - \Phi^t)/\Phi^t \times 100\%$, where Φ^m and Φ^t are the measured and the theoretical work function values, respectively. The measured Ag work function shows a good agreement with the theoretical value, which validates the reliability of the tip work function value of 4.52 eV. Actually, the measured tip work function of 4.52 eV is also consistent with n-Si theoretical value of 4.43 eV with the average error less than 2.0%. Therefore, we consider that the experimental error is in the acceptable scope. Based on the Eq. (5), the work function of olivine surface is given by

$$\Phi_{ol} = \Phi_{HOPG} - Q(V_{CPD_{HOPG-tip}} - V_{CPD_{ol-tip}}) \tag{6}$$

where $V_{CPD_{ol-tip}}$ is the measured contact potential difference between the olivine surface and the tip. Additionally, for accurately obtaining the work function values, the sample surface was previously polished with the 1.5 μm diamond powder and cleared by absolute ethyl alcohol. All data and images are acquired under the UHV condition for more truly simulating the space environment. Under this condition, the effect of surface absorption on the work function of sample surface is negligible.

3. Results and discussion

3.1. Results

As shown in Table 1, we summarized the work function values of the 15 scanning areas derived from contact potential difference measurements. Noting that Z is the tip position and B is the local bias, as shown in the second and the third columns, respectively. The tip position Z is adjusted to zero by the Auto button in the Z-Controller before the first sample surface scanning, and Z scan range of tip is ± 600 nm in KPFM module, which means surface morphology within the range of ±600 nm able to be measured.

Table 1
Work functions of olivine derived from contact potential difference measurements.

No.	Z (nm)	B (mV)	CPD (V)	Work function (eV)
01	(−14.9, 17.5)	(−285, 316)	3.104	7.624 ± 0.027
02	(−14.8, 7.4)	(−59, 63)	3.623	8.143 ± 0.009
03	(−20.6, 10.5)	(−53, 72)	3.702	8.222 ± 0.010
04	(−20.0, 11.5)	(−73, 85)	3.929	8.449 ± 0.010
05	(−19.8, 19.5)	(−136, 131)	3.249	7.769 ± 0.026
06	(−25.7, 45.8)	(−333, 348)	3.598	8.118 ± 0.047
07	(−33.9, 25.5)	(−174, 163)	3.059	7.579 ± 0.032
08	(−21.7, 49.9)	(−246, 207)	3.508	8.028 ± 0.053
09	(−51.7, 33.0)	(−256, 217)	2.784	7.304 ± 0.039
10	(−34.2, 35.6)	(−502, 471)	2.798	7.318 ± 0.099
11	(−28.4, 37.3)	(−158, 194)	3.252	7.772 ± 0.034
12	(−41.2, 31.0)	(−501, 575)	3.653	8.173 ± 0.109
13	(−51.9, 50.6)	(−306, 448)	3.770	8.290 ± 0.055
14	(−47.7, 52.4)	(−345, 372)	3.555	8.075 ± 0.052
15	(−71.2, 84.8)	(−551, 469)	3.176	7.696 ± 0.075
mean	–	–	3.384	7.900 ± 0.345

The local bias B is the potential difference between the scanning point and the tip after the CPD was compensated. CPD represents the compensated potential, as shown in the fourth column, which approximately equals to the average contact potential difference between the AFM tip and the scanning area on the sample surface. Therefore, the local work function values are determined by

$$\Phi_{ol}^{local} = \Phi_{HOPG} - Q(V_{CPD_{HOPG-tip}} - V_{CPD_{ol-tip}}) + B \quad (7)$$

The mean of the local work function values are presented in the last column. The values after the ± sign are the standard deviations of each scanning area.

Fig. 1 shows the measured results derived from the last column of Table 1. All the values were acquired from different scanning areas on the same surface of an olivine sample. Each target area was scanned at least twice, and it costs more than one hour. In the first scanning, surface morphology with the area of $3 \times 3\ \mu m^2$ or $5 \times 5\ \mu m^2$ was obtained. But in the second scanning, the bias and surface morphology with the area of $1 \times 1\ \mu m^2$ were simultaneously acquired with resolution of 256×256 pixels from the first morphology image. Repeated scanning method was performed to verify the reproducibility of our measurements. However, it is difficult to scan repeatedly the same area of $1 \times 1\ \mu m^2$ on the sample surface. As shown in Fig. 1, we measured 15 times on the same surface of the olivine sample. Each diamond indicates the average work function of the scanning area and the error bars are respectively defined to be one standard deviation above and below the mean of the $1 \times 1\ \mu m^2$ scanning area. Obviously, the measured work function of each scanning area is quite stable, except the Nos. 10 and 12 areas which present the relative greater variation range of about 0.1 eV. This may be related to the effect of scratches which will be discussed in the following context.

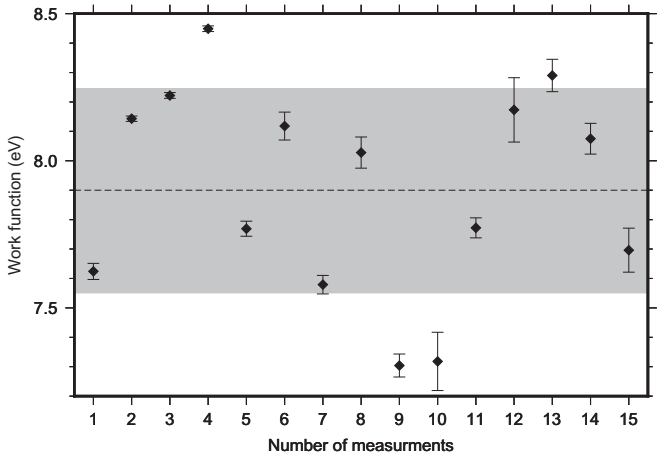

Fig. 1. Work function measurements on the different scanning areas of olivine mineral surface. The diamonds indicate the mean of the local work function and the error bars of each measurement denote the standard deviation of every scanning area on the sample surface. The black dashed line indicates the mean work function (7.9 eV) of the 15 scanning areas and the light gray area is the variation region of one standard deviation (0.345 eV) above and below the mean.

Additionally, the black dashed line indicates the mean work function of 7.900 eV for the 15 target areas and the gray area denotes the variation region of the standard deviation (0.345 eV) above and below the mean. As expected, the measured work function values vary along the mean value within the standard deviation except the Nos. 4, 9, 10, and 13 measurements. It indicates that the measured work function in different areas of olivine mineral is relatively stable and our measurements show a good reproducibility. The measurements of Nos. 4, 9, 10, and 13 may be attributed to the olivine crystal orientation. As in the above analysis, we derived the value 7.900 eV can be taken as the average work function of olivine mineral surface and the measured work function is 7.900 ± 0.345 eV based on repeated measurements.

3.2. Effects of surface morphology and crystal orientation

As noted above, the surface morphology plays an important role in measured bias or work function. Fig. 2 shows the relations of the measured bias (a) and work function (b) with surface morphology. In order to characterize the effect of surface morphology on our measurements, here, we employed a linear fitting method (red lines) as an example for better interpreting our data. Note that the parameters presented in Fig. 2 may not be de facto linear relations. As shown in Fig. 2(a), the maximum difference of bias (ΔB) tends to increase gradually with increase of the maximum surface height difference (ΔZ). It indicates that drastic changing of surface height such as small bumps or depressions would cause great bias variations. Hence, the work function derived from bias may also present great variations as a result of surface height changing. To compare the morphology of different scanning areas, here we used the standard deviation of height (σ_Z) to characterize the micro-roughness of the sample surface. As shown in Fig. 2(b), the standard deviation of work function (σ_{WF}) apparently tends to be greater with the increasing of σ_Z. That is, the measured work function becomes more reliable and stable for less coarser scanning target.

For further analyzing the effect of surface morphology on the work function, as an example, Fig. 3 shows two $1 \times 1\ \mu m_2$ scans of simultaneously acquired bias and surface morphology of olivine sample surface, which corresponds to the data of No. 09 of Table 1. The left panel shows the bias image, and the bias difference is 473 mV. The right panel shows the surface morphology of the olivine sample, and the height difference is 84.7 nm. On the whole, the bias exhibits a well correlation with the surface morphology, especially the nearly parallel scratches. In order to contrast the bias with morphology, we selected four profile lines (a–d) in the scanning area, as an example shown in Fig. 4.

As shown in (a) and (b), the bias values mostly have been scaled between −50 mV and 50 mV and the corresponding height range is limited to (−5, 5) nm. Interestingly, for the relatively smooth surface, the bias tends to

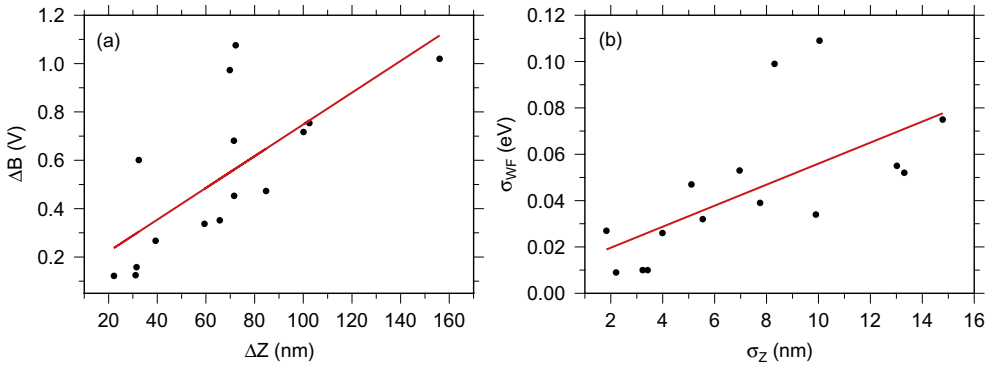

Fig. 2. Effects of surface morphology on the bias and the work function. (a) Scatter plot of the maximum bias difference (ΔB) versus the maximum height difference (ΔZ); (b) Scatter plot of standard deviation of work function (σ_{WF}) versus that of altitude (σ_Z). The red lines are acquired by a linear fitting method. (For interpretation of the references to colour in this figure legend, the reader is referred to the web version of this article.)

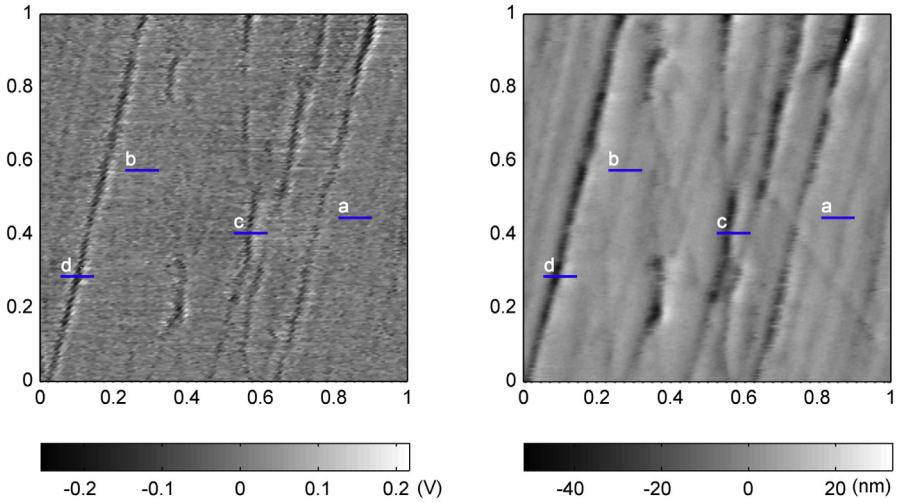

Fig. 3. Shown are the measured 1 ×1 μm^2 (256 × 256 pixels) bias (left) and morphology (right) of the olivine surface under UHV condition. The profile lines (a–d) denote the analysed lines as examples.

be anti-correlated with the sample surface altitude, as shown in (a) and (b). According to the surface gap state theory, the predominantly exposing olivine surface has a lower surface work function due to the existence of surface dipole layer caused by the surface morphology. However, the bias range caused by the height variation within several nanometers scale is about the same order of magnitude as the standard deviation of 0.039 eV. Therefore, the effect of surface morphology with the variation range of a few nanometers is negligible.

However, the effect of surface morphology on the work function values near those scratches is very significant. As shown in (c) and (d), the maximum bias difference reaches up to about 400 mV and the maximum height difference is roughly 50 nm over the two scanning lines. The altitude outside the range of (−5, 5) nm is attributed to the scratches, which corresponds to the bias values of <−50 mV and >50 mV. In fact, for the 15 scanning areas, the bias would fluctuate in excess of the range of (−50, 50) mV that corresponds to the drastically changing morphology at the scratches. This confirms that the measured bias of olivine is significantly affected by the scratches, especially for the slopes edges. As shown in Fig. 4(c) and (d), the bias changes across the slope and appears the local maximum values on the downslope side of the scratch and the local minimum values on the upslope of the scratch. This phenomenon also indicates that the surface morphology plays an important role in the accurate measurement of the surface work function (Li and Li, 2005). The reason of the larger bias range is probably due to the effect of slopes on the tip wall, as well as the slope morphology. For the diversity and complexity of surface morphology, therefore, we consider the mean measurements of olivine work function in the relatively smooth scanning area as the reasonable work function value, as shown in the last column of Table 1.

However, the mean work function values of different target areas fluctuate in the range of ±0.6 eV, as shown in Fig. 1. All the values of olivine work function are acquired from the 15 different scanning areas on the same sample surface by KPFM. The great variation of the measured work function from 7.3 eV to 8.5 eV may be

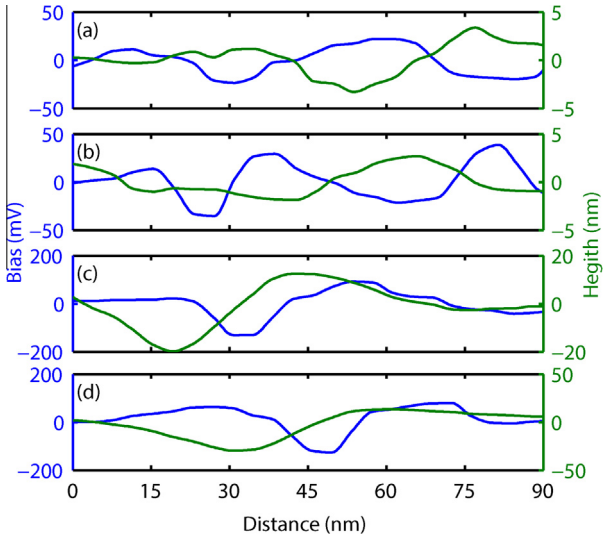

Fig. 4. Profile lines of morphology (green) and bias (blue) of olivine measured by KPFM. (a) and (b) were chose from the relatively smooth surface, but (c) and (d) respectively crossed a scratch. (For interpretation of the references to colour in this figure legend, the reader is referred to the web version of this article.)

attributed to crystal orientation. Olivine is a type of nesosilicate minerals. There is difference of the atomic arrangement among different crystal faces. Work function of solid materials is strongly dependent on the arrangement of the outermost atoms on the solid surface. Therefore, work function of the olivine crystal face with the closest packing arrangements of surface atoms remains higher than that of other faces. That is, anisotropy of olivine crystal is so significant that work function values measured from different crystal faces of olivine vary in a certain range. Therefore, the measured work function values of 15 target areas may characterize the photoemission charging properties of the different crystal faces of olivine mineral. The effect of crystal orientation on the work function need to be further investigated in future work.

3.3. Photoemission charging properties of olivine

According to Einstein's photoelectric equation, the maximum energy of photoelectron is decided by

$$E_k = h\nu - \Phi = h\frac{c}{\lambda} - \Phi \tag{8}$$

where h is the Planck constant, ν is the frequency of the incident photon and $h\nu$ is the photon energy. Φ is the work function of material surface. c and λ are the velocity of light in a vacuum and its wavelength, respectively. The minimum photon energy required in photoemission needs only satisfy $h\nu > \Phi$, if the photoelectron energy is low enough. Therefore, the photoemission will occur only if the frequency of the incident photon is greater than the threshold frequency; or the wavelength of the incident photon should be lower than the threshold wavelength. Based on Eq. (8), the threshold wavelength of olivine ejecting a photoelectron is 171 nm. It indicates that electron was emitted from the surface of olivine under X-ray and solar ultraviolet irradiation with wavelength of <171 nm.

The total photoelectron flux tends to lower, since the solar irradiation flux rapidly decreases in ultraviolet wavelength bands. However, the silicate mineral, typical olivine in the mafic lunar mare, for example, is a good insulator, enduring two weeks long time insolation in a diurnal day. As a result, the regolith continually accumulates charge enough with very few charge transfer and decay in lunar vacuum environment for the extremely low electrical conductivity. This photoemission charging process of lunar regolith is mainly responsible for creating the global-scale electrostatic field on lunar day side. Driven by electrostatic field, the charged fines levitate and even cause the horizon glow by scattering the sunlight as observed by Surveyor, Apollo and Clementine etc. (Rennilson and Criswell, 1974; Berg et al., 1976; Zook et al., 1995). For further understanding the charging process of regolith materials induced by photoemission, we would like to measure and compare photoemission charging properties of more ubiquitous silicate minerals in space, such as pyroxene and feldspar, in future study.

4. Conclusions

Work function is a fundamental physical characteristic of solid material surface. The photoemission charging of dust grains in lunar atmosphere or space plasma environments as well as the formation of electrostatic field on lunar sunlit surface creates a growing demand to investigate the photoemission charging properties of insulator mineral, which is related to the work function of mineral surface. KPFM was demonstrated to be a powerful tool for the work function investigation of mineral material surface. In this paper, KPFM was applied for the measurement of the contact potential difference and the estimation of the local work function on the heterogeneous olivine samples. Our results showed that the work function of olivine falls within a range of 7.3–8.5 eV, which indicated insulator mineral, olivine, can absorb energy from solar ultraviolet and X-ray irradiation with wavelength of <171 nm in space environment and emit photoelectron from olivine surface. Additionally, based on a dozen scanning areas on the surface of olivine, we found that the bias exhibited a well anti-correlation with the surface morphology and is significantly influenced by crystal orientation. In future work, the work function measurements of pyroxene, plagioclase and ilmenite will be performed with KPFM, which may contribute to the understanding of lunar dust charging and transport, and the development of the electrostatic beneficiation and the dust mitigation technology.

Acknowledgements

The authors thank Yang Li, Bing Mo and Xiaojia Zeng for their support and experimental assistance of this study.

This work was supported by the National Natural Science Foundation of China (General Program: No. 41373067, 41572037; Major Program: No. 41490630), the Macau FDCT program (020/2014/A1), Youth Innovation Promotion Association of CAS (2014359) and the pre-research project of GAD(060402).

References

Berg, O.E., Wolf, H., Rhee, J., 1976. Lunar soil movement registerd by the apollo 17 cosmic dust experiment. In: Interplanetary Dust and Zodiacal Light. Springer, pp. 233–237.

Colwell, J., Batiste, S., Horányi, M., Robertson, S., Sture, S., 2007. Lunar surface: dust dynamics and regolith mechanics. Rev. Geophys. 45 (2), RG2006.

Delory, G.T., 2010. Electrical phenomena on the moon and mars. In: Proc. ESA Annual Meeting on Electrostatics. p. 2.

Ekardt, W., 1984. Work function of small metal particles: self-consistent spherical jellium-background model. Phys. Rev. B 29 (4), 1558.

Feuerbacher, B., Anderegg, M., Fitton, B., Laude, L., Willis, R., Grard, R., 1972. Photoemission from lunar surface fines and the lunar photoelectron sheath. In: Lunar and Planetary Science Conference Proceedings, vol. 3. p. 2655.

Freeman, J., Ibrahim, M., 1975. Lunar electric fields, surface potential and associated plasma sheaths. Earth Moon Planets 14 (1), 103–114.

Fujii, R., Gotoh, Y., Liao, M., Tsuji, H., Ishikawa, J., 2006. Work function measurement of transition metal nitride and carbide thin films. Vacuum 80 (7), 832–835.

Gallo, C., Lama, W., 1976. Classical electrostatic description of the work function and ionization energy of insulators. Ind. Appl. IEEE Trans. 1, 7–11.

Gallo, C., Lama, W., 1976. Some charge exchange phenomena explained by a classical model of the work function. J. Electrostat. 2 (2), 145–150.

Grobman, W.D., Blank, J.L., 1969. Electrostatic potential distribution of the sunlit lunar surface. J. Geophys. Res. 74 (16), 3943–3951.

Gupta, R., Gidaspow, D., Wasan, D., 1993. Electrostatic separation of powder mixtures based on the work functions of its constituents. Powder Technol. 75 (1), 79–87.

Hoppe, H., Glatzel, T., Niggemann, M., Hinsch, A., Lux-Steiner, M.C., Sariciftci, N., 2005. Kelvin probe force microscopy study on conjugated polymer/fullerene bulk heterojunction organic solar cells. Nano Lett. 5 (2), 269–274.

Kim, C.H., Bae, C.D., Ryu, K.H., Lee, B.K., Shin, H.J., 2007. Local work function measurements on various inorganic materials using kelvin probe force spectroscopy. In: Solid State Phenomena, vol. 124. Trans Tech Publ, pp. 607–610.

Kim, J., Lägel, B., Moons, E., Johansson, N., Baikie, I., Salaneck, W.R., Friend, R., Cacialli, F., 2000. Kelvin probe and ultraviolet photoemission measurements of indium tin oxide work function: a comparison. Synt. Metals 111, 311–314.

Kotani, M., Akamatu, H., 1971. Contact potential difference and work function of organic crystals. Disc. Faraday Soc. 51, 94–101.

Kötz, E., Neff, H., Müller, K., 1986. A ups, xps and work function study of emersed silver, platinum and gold electrodes. J. Electroanal. Chem. Interfacial Electrochem. 215 (1), 331–344.

Lang, N., Kohn, W., 1971. Theory of metal surfaces: work function. Phys. Rev. B 3 (4), 1215.

Li, T.X., Ban, H., Hower, J.C., Stencel, J.M., Saito, K., 1999. Dry triboelectrostatic separation of mineral particles: a potential application in space exploration. J. Electrostat. 47 (3), 133–142.

Li, W., Li, D., 2005. On the correlation between surface roughness and work function in copper. J. Chem. Phys. 122 (6), 064708.

Manka, R.H., 1973. Plasma and potential at the lunar surface. In: Photon and Particle Interactions with Surfaces in Space. Springer, pp. 347–361.

Melitz, W., Shen, J., Kummel, A.C., Lee, S., 2011. Kelvin probe force microscopy and its application. Surf. Sci. Rep. 66 (1), 1–27.

Nonnenmacher, M., O'Boyle, M., Wickramasinghe, H., 1991. Kelvin probe force microscopy. Appl. Phys. Lett. 58 (25), 2921–2923.

Park, Y., Choong, V., Gao, Y., Hsieh, B., Tang, C., 1996. Work function of indium tin oxide transparent conductor measured by photoelectron spectroscopy. Appl. Phys. Lett. 68 (19), 2699–2701.

Reasoner, D.L., Burke, W.J., 1972. Characteristics of the lunar photoelectron layer in the geomagnetic tail. J. Geophys. Res. 77 (34), 6671–6687.

Rennilson, J.J., Criswell, D.R., 1974. Surveyor observations of lunar horizon-glow. Earth Moon Planets 10 (2), 121–142.

Sadewasser, S., Glatzel, T., Rusu, M., Jäger-Waldau, A., Lux-Steiner, M. C., 2002. High-resolution work function imaging of single grains of semiconductor surfaces. Appl. Phys. Lett. 80 (16), 2979–2981.

Sadewasser, S., Jelinek, P., Fang, C.-K., Custance, O., Yamada, Y., Sugimoto, Y., Abe, M., Morita, S., 2009. New insights on atomic-resolution frequency-modulation kelvin-probe force-microscopy imaging of semiconductors. Phys. Rev. Lett. 103 (26), 266103.

Sickafoose, A., Colwell, J., Horɕnyi, M., Robertson, S., 2001. Experimental investigations on photoelectric and triboelectric charging of dust. J. Geophys. Res. 106 (5), 8343–8356.

Sickafoose, A.A., Colwell, J.E., Horɕnyi, M., Robertson, S., 2000. Photoelectric charging of dust particles in vacuum. Phys. Rev. Lett. 84 (26), 6034–6037.

Sommerhalter, C., Matthes, T.W., Glatzel, T., Jäger-Waldau, A., Lux-Steiner, M.C., 1999. High-sensitivity quantitative kelvin probe microscopy by noncontact ultra-high-vacuum atomic force microscopy. Appl. Phys. Lett. 75 (2), 286–288.

Sternovsky, Z., Chamberlin, P., Horɕnyi, M., et al., 2008. Variability of the lunar photoelectron sheath and dust mobility due to solar activity. J. Geophys. Res. 113 (A10).

Zook, H., Potter, A., Cooper, B., 1995. The lunar dust exosphere and clementine lunar horizon glow. In: Lunar and Planetary Science Conference, vol. 26. p. 1577.